EurJIC European Journal of Inorganic Chemistry
ChemPubSoc Europe
FULL PAPER

DOI:10.1002/ejic.201402593

Defining the Structural Parameters of Triazole Ligands in the Templated Synthesis of Silver Nanoparticles

Heba A. Kashmery,[a] Alasdair W. Clark,[b] Ruggero Dondi,[c] Andrew J. Fallows,[d] Paul M. Cullis,[d] and Glenn A. Burley*[a]

Keywords: Template synthesis / Nanoparticles / Silver / Click chemistry / Nitrogen heterocycles

This manuscript describes a one-pot method for the synthesis of size- and shape-selected silver nanoparticles (AgNPs) using Tollens' reagent [$Ag(NH_3)_2OH$] as the silver source. Sugar triazole ligands facilitate the formation of monodisperse AgNPs in which the size and shape can be controlled according to the reaction conditions. Increasing the size of the ligand reduces size tunability but enhances colloidal stability in high-salt buffers. A key conclusion from this study is that the Ag^I-binding affinity of these triazole ligands determines their capacity to tune the size of the resultant AgNPs formed. Weaker Ag^I-binding ligands can be used to form monodisperse, angular AgNPs over a wider range of sizes [(12 ± 3) to (33 ± 7) nm], whereas triazole ligands that exhibit a higher Ag^I-binding affinity produce monodisperse, spherical AgNPs of a single size [(18 ± 5) nm].

Introduction

Silver nanoparticles (AgNPs) are of considerable importance for the development of highly sensitive plasmon-based diagnostic platforms.[1] By virtue of their strong surface plasmon resonance that can extend throughout the visible and near-infrared regions,[2,3] AgNPs are superior plasmonic candidates relative to other noble-metal nanoparticles such as gold and copper.[4–8] Although a variety of methods exist for the preparation of AgNPs,[9,10] very few of these can control both the size and shape of AgNPs under mild reductive conditions and at room temperature.[11–13] AgNP formation using Tollens' reagent [$Ag(NH_3)_2OH$] in the presence of aldehydes is one such method that has been underutilised in the literature.[11,14–16] Monosaccharides and disaccharides have been used previously to form AgNPs with varying levels of dispersity and colloidal stability.[17–22] Despite the simple method of preparation of AgNPs and mild reaction conditions of this process, an in-depth understanding of the mechanistic factors that control AgNP formation using Tollens' reagent is lacking.

To address this shortfall, we have explored the use of Ag^I-binding triazole ligands to direct the synthesis of size- and shape-selected AgNPs using Tollens' reagent.[23] In an earlier study, we reported the utility of the Ag^I-binding ligand **1** [Figure 1 (a)] to form monodisperse and stable suspensions of spherical AgNPs [i.e., AgNP@(**1**)]. Our current mechanistic rationale for the formation of AgNP@(**1**) involves the initial coordination of Ag^I to the 3-position (N^a) of both the resorcinol triazole nitrogen atoms [red in Figure 1 (a)] and the 2-position (N^b) of the southern-most triazole nitrogen atom [pink in Figure 1 (a)]. We surmised that the chelating effect of **1** positions Ag^I atoms in close proximity to the aldehyde groups of the galactose sugars. Once in position, these sugars facilitate the reduction of Ag^I to putatively form nanoclusters of Ag nuclei.[24] These chelated nanoclusters can then form size-selected AgNPs by an exponential growth phase followed by termination and ligand capping [Figure 1 (a)].[16,25] What was unclear from our previous work was how each of the constituent structural elements (i.e., sugar unit, triazole, aromatic core) influenced the size and dispersity of AgNP formation.

Kvitek et al. proposed a correlation between the molecular structure of the reducing sugars used in the Tollens-mediated formation of AgNPs.[21] Disaccharides (e.g., maltose), for example, produced smaller AgNPs with a narrower size distribution relative to monosaccharides (e.g., glucose). The justification given by the authors for this observation was that disaccharides had an increased number of reducing

[a] Department of Pure & Applied Chemistry, University of Strathclyde,
295 Cathedral Street, Glasgow, G1 1XL, UK
E-mail: glenn.burley@strath.ac.uk
http://www.burleylabs.co.uk
http://www.strath.ac.uk/chemistry/staff/academic/glennburley/
[b] Division of Biomedical Engineering, School of Engineering, University of Glasgow,
Oakfield Avenue, Glasgow, G12 8LT, UK
[c] Department of Pharmacy and Pharmacology,
University of Bath, Claverton Down,
Bath, BA2 7AY, UK
[d] Department of Chemistry, University of Leicester,
University Road, Leicester, LE1 7RH, UK
Supporting information for this article is available on the WWW under http://dx.doi.org/10.1002/ejic.201402593.

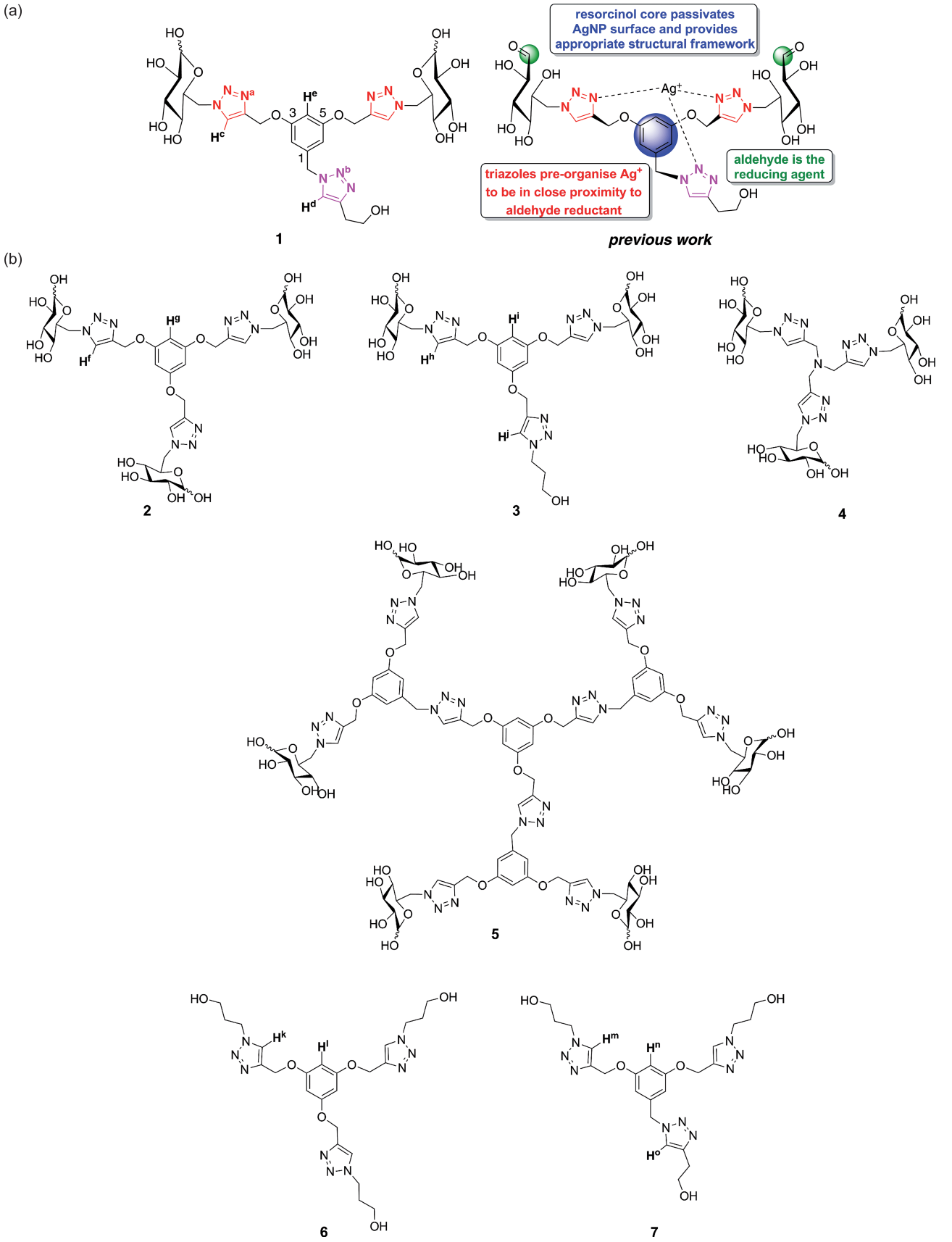

Figure 1. (a) Proposed binding model of the templated synthesis of AgNPs using the first-generation ligand **1**. (b) Structures of sugar triazoles **2**–**7** prepared in this study.

equivalents relative to monosaccharides.[20] This observation is in contrast to our previous study,[23] in which we showed that an increase in the number of reducing equivalents (i.e., increasing the number of reducing sugar units from two of **1** to four) did not result in the formation of smaller AgNPs.

These somewhat conflicting observations have led us to hypothesise that the Ag^I binding affinity of our triazole ligands rather than the number of reducing sugars could be playing a defining role in influencing the size of the resultant AgNPs formed.[26] In this manuscript, we show that the structure of the ligand determines the size, shape, dispersity and stability of these AgNPs. We also show that weaker Ag^I-binding ligands enable access to monodisperse AgNPs where their size can be tuned according to the reaction conditions used. Finally, we show evidence that an increase in the Ag^I-binding affinity of ligands produces AgNPs smaller in diameter.

Results

Design of Sugar Triazole Ligands 2–7

In our first-generation ligand design (e.g., **1**), a central resorcinol scaffold was used to tether two galactose sugar units by means of a triazole linkage.[23] A third triazole with different regiochemistry to the two resorcinol triazoles was installed in the southern part of **1** to complete a three-triazole ligand structure. The underlying motivation for exploring this original design was based on a previous observation that this ligand was used to form Ag nanostructures when covalently attached to DNA duplexes and exposed to Tollens' reagent.[27] To gain further insight into how the ligand structure could influence AgNP formation, ligands were prepared in which the resorcinol core (as present in **1**) was replaced with phloroglucinol [Figure 1 (b)]. This change subtly alters the triazole regiochemistry and inter-triazole distance in the southern part of the ligand. The influence of this change on AgNP formation was investigated using a three-sugar triazole (**2**) and two-sugar triazole (**3**) ligand system. The role of the central aromatic ring was probed by the replacement of the resorcinol core with a central nitrogen atom (**4**). To further explore how sugar density plays a role in the size and shape of AgNPs, the hybrid ligand (**5**) was synthesised. Finally, to investigate how the Ag^I-binding affinity is influenced by the galactose sugar units, compounds **6** and **7** were prepared.

Synthesis of Sugar Triazole Ligands 2–7

Sugar triazole **2** was prepared from phloroglucinol (1,3,5-trihydroxybenzene) (**8**) in three steps (Scheme 1). Alkylation of **8** with propargyl bromide afforded **9** in 40% yield.[28] The formation of **11** proceeded smoothly under standard copper-catalysed Huisgen cycloaddition conditions using four equivalents of galactose azide **10**. Acid de-

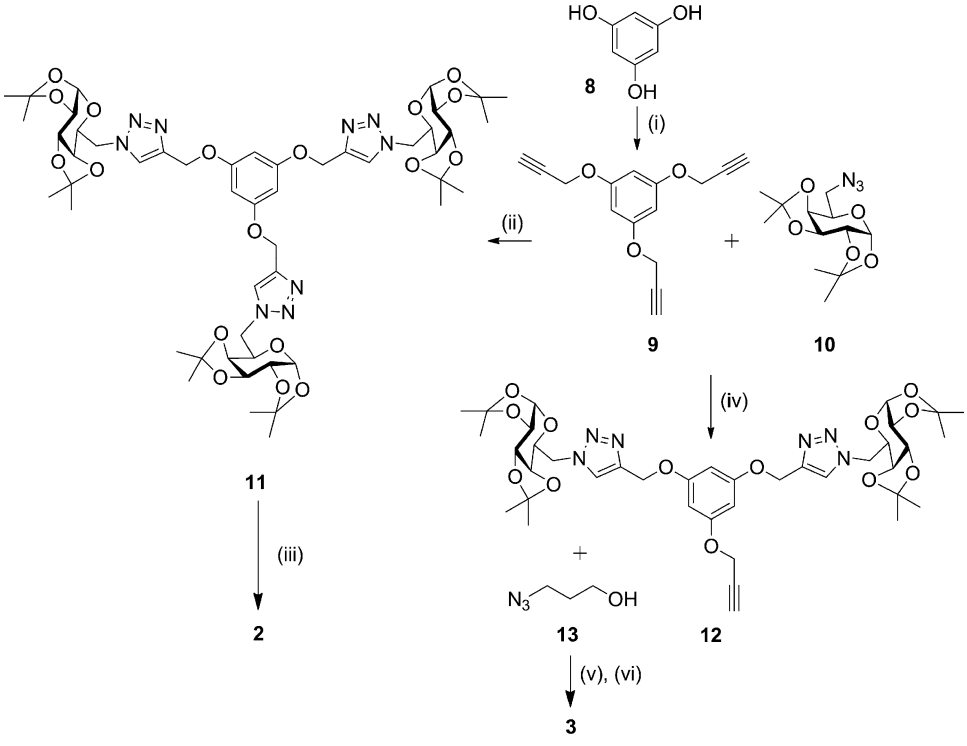

Scheme 1. Preparation of **2** and **3**. Reagents and conditions: (i) Propargyl bromide (3.5 equiv.), K_2CO_3 (3.5 equiv.), 18-crown-6 (0.2 equiv.), CH_3CN, reflux, 24 h, 40%; (ii) compound **10** (4.0 equiv.) $CuSO_4$ (0.1 M, 0.32 equiv.), sodium ascorbate (2.0 equiv.), THF/H_2O (3:1), 67%; (iii) trifluoroacetic acid (TFA)/H_2O (1:1), 70 °C, 3 h, 60%; (iv) compound **10** (2.0 equiv.), $CuSO_4$ (0.1 M, 0.34 equiv.), sodium ascorbate (2.0 equiv.), THF/H_2O (3:1), 24%; (v) ligand **13** (5.0 equiv.), $CuSO_4$ (0.1 M, 1.2 equiv.), sodium ascorbate (2.0 equiv.), THF/H_2O (3:1); and (vi) TFA/H_2O (1:1), reflux, 70 °C, 3 h, 70% over two steps.

protection of the isopropylidene groups of **11** afforded **2** after purification by means of reverse-phase (RP)-HPLC. For the synthesis of compound **3**, a twofold click reaction between **9** and **10** afforded **12** in 24% yield. A third click reaction using 3-azido-1-propanol (**13**) followed by acid deprotection of the isopropylidines and purification by RP-HPLC yielded **3**.

Sugar triazole **4** was prepared by a threefold click reaction between commercially available tripropargylamine (**14**) and galactose azide (**10**), followed by acid deprotection and purification by RP-HPLC (Scheme 2). Compound **5** was prepared in a convergent manner through triazole formation by using **9** and **15** (3.3 equiv.) in the presence of copper(I) to initially yield **16** in 41% yield, followed by acid deprotection of the isopropylidine groups to afford **5** (Scheme 3).

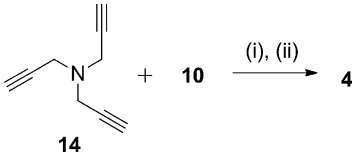

Scheme 2. Preparation of **4**. Reagents and conditions: (i) Compound **10** (4.5 equiv.), 2,6-lutidine (1.0 equiv.), $[Cu(CH_3CN)_4]PF_6$ (0.01 equiv.), CH_3CN, 0 °C, 36%; and (ii) TFA/H_2O (1:1), 70 °C, 3 h, 60%.

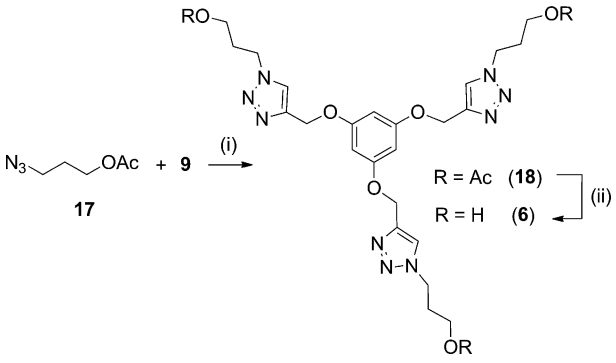

Scheme 4. Preparation of **6**. Reagents and conditions: (i) Compound **17** (5.1 equiv.), $CuSO_4$ (0.1 M, 0.33 equiv.), sodium ascorbate (2.0 equiv.), THF/H_2O (3:1), 24 h; and (ii) ammonia in methanol (2 M), reflux, 40 °C, 24 h, 50% over two steps.

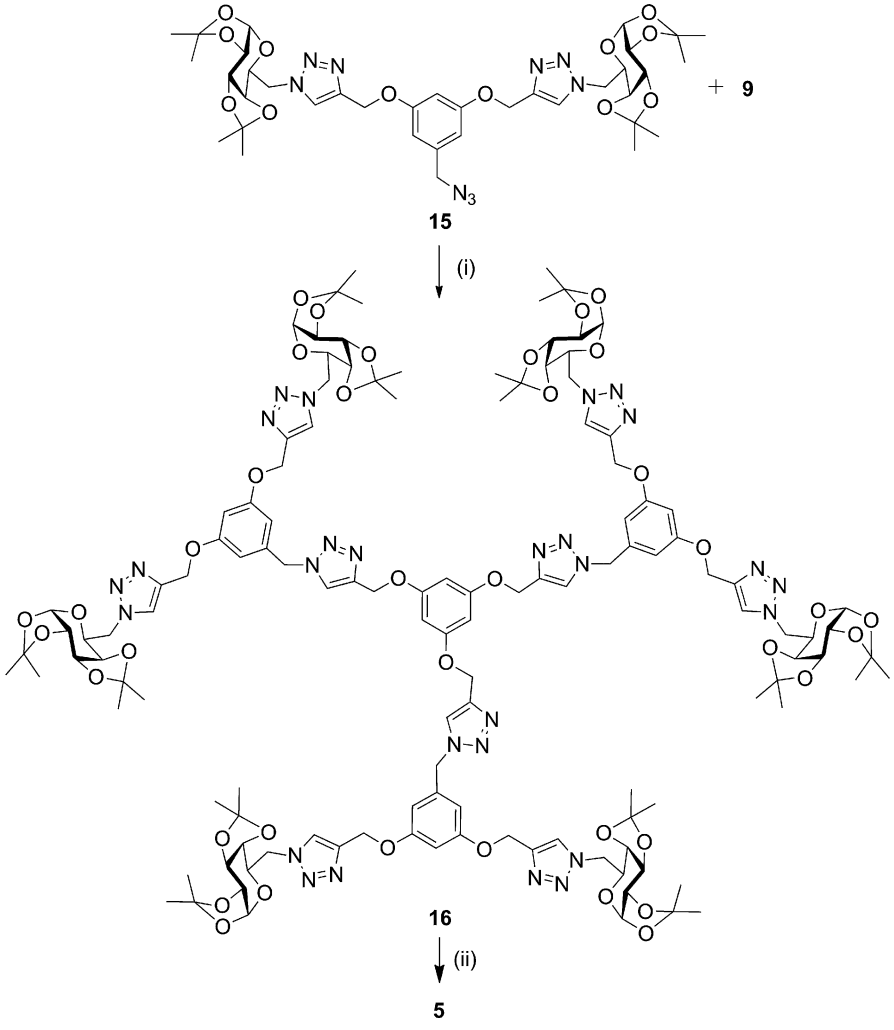

Scheme 3. Preparation of **5**. Reagents and conditions: (i) Compound **15** (3.3 equiv.), $CuSO_4$ (0.1 M, 1.48 equiv.), sodium ascorbate (2.0 equiv.), THF/H_2O (3:1), 24 h, 41%; and (ii) TFA/H_2O (1:1), 70 °C, 24 h, 47%.

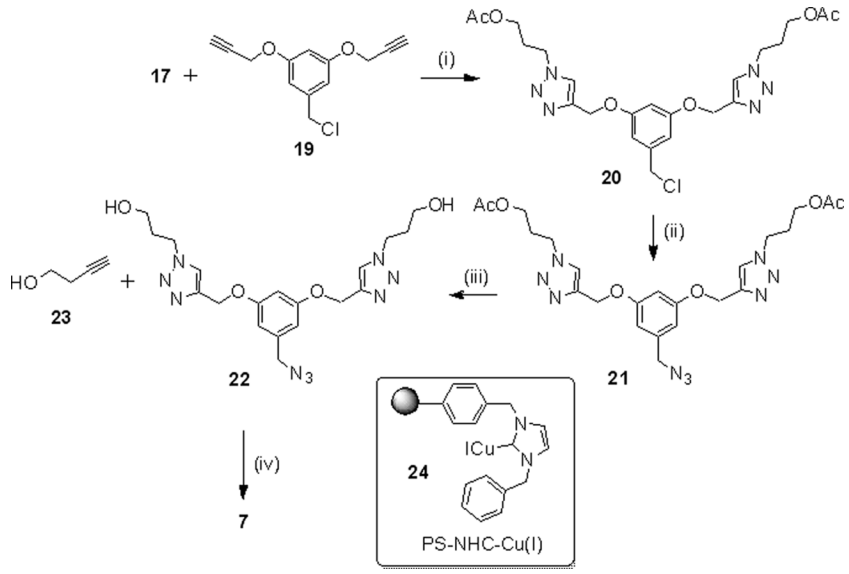

Scheme 5. Preparation of **7**. Reagents and conditions: (i) Compound **17** (3.0 equiv.), $CuSO_4$ (0.1 M, 0.33 equiv.), sodium ascorbate (2.0 equiv.), THF/H_2O (3:1), 24 h, 76%; (ii) NaN_3 (10.0 equiv.), acetone/H_2O (4:1), reflux, 3 h, 85%; (iii) ammonia in methanol (2 M), reflux, 40 °C, 24 h; and (iv) compound **23** (3.0 equiv.), compound **24** (1.1 equiv.), DMSO, room temperature, 24 h, 31% over two steps.

Triazole ligand **6** was prepared by a click reaction between azide **17** and alkyne **9**. Base-mediated acetyl deprotection and purification by RP-HPLC afforded the trihydroxylated ligand **6** in 50% yield (Scheme 4). Finally, ligand **7** was prepared by triazole formation between **19** and **17** (3 equiv.) in the presence of copper(I) to yield **20**. Chloride displacement of **20** using NaN_3 yielded azide **21**. Deprotection of the acetyl groups of **21** with ammonia produced the dihydroxylated compound **22**. The installation of the southernmost triazole group was achieved by a click reaction between **22** and butyn-1-ol **23** using resin-bound Cu^{I}[29] (**24**) in 31% yield (Scheme 5). Immobilisation of Cu^{I} was critical for the isolation of pure ligand **7** as conventional click chemistry conditions resulted in a significant amount of **7** complexed with copper.

Ligands 2–5 Templated the Formation of Angular AgNPs

The formation of AgNPs was screened as a function of [ligand] and [Tollens']. A reaction screen of [**2**] and [Tollens'] produced AgNP@(**2**) in three regions [yellow boxes in Figure 2 (a)]: (i) A region of low concentration of Tollens' (i.e., 1 mM); (ii) a region of intermediate concentration of Tollens' (10 mM); and (iii) lastly, a high concentration region of Tollens' (20 to 50 mM). The dependence on concentration of both ligand and Tollens' was similar to AgNPs derived from **1** (i.e., AgNP@**1**).[23] Silver aggregates were also observed in some reaction vessels [grey boxes, Figure 2 (a)]. UV/Vis spectra of AgNP@**2** formed in these three exemplar regions all exhibited a diagnostic surface plasmon resonance peak at approximately 420 nm [Figure 2 (b)]. TEM analysis revealed that AgNP@**2** formed angular AgNPs of similar diameter (Figure 3). For example, #15 (lower concentration of Tollens') and #31 (high concentration of Tollens') afforded angular AgNP@**2** with diameters of (21 ± 3) and (18 ± 5) nm, respectively. AgNP@**2** formed using an intermediate concentration of Tollens' (i.e., #19), produced AgNPs [Ø = (17 ± 3) nm]. These AgNPs were larger in diameter and of different shape than AgNP@**1** [Ø = (8 ± 5) nm].[23]

(a)

[(2)]

[Tollens']

	25mM	10mM	1mM	100µM	10µM	1µM
10µM	#1	#2	#3	#4	#5	#6
100µM	#7	#8	#9	#10	#11	#12
1mM	#13	#14	#15 21 ± 3 nm	#16	#17	#18
10mM	#19 17 ± 3 nm	#20	#21	#22	#23	#24
20mM	#25	#26	#27	#28	#29	#30
50mM	#31 18 ± 5 nm	#32	#33	#34	#35	#36

(b)

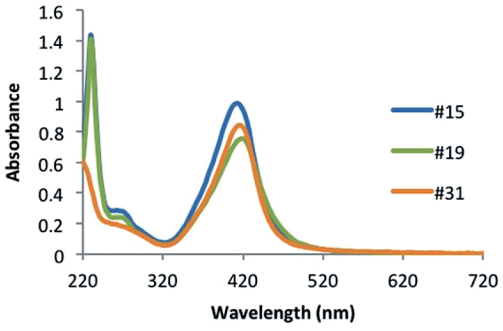

Figure 2. (a) AgNP screening array prepared using sugar triazole **2** and Tollens' reagent. White boxes represent no AgNP formation, yellow boxes represent AgNP formation and grey boxes represent the formation of silver mirrors. (b) UV/Vis spectra of reactions #15, 19 and 31, which formed AgNPs as observed by a surface plasmon peak at 420 nm. Sample #19 was diluted 1:10 and #31 was diluted 1:70 prior to the measurements.

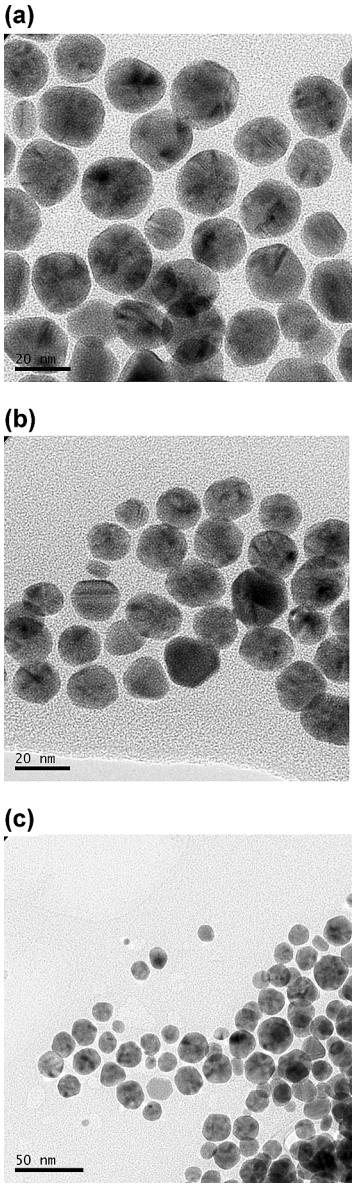

Figure 3. TEM images of AgNP@**2** prepared using reaction conditions in Figure 2 (a): (a) #15, Ø = (21 ± 3) nm. (b) #19, Ø = (17 ± 3) nm. (c) #31, Ø = (18 ± 5) nm.

The formation of AgNPs was then investigated using ligand **3**. AgNP@**3** was formed over concentration ranges of 1 to 25 mM [**3**] and 10 to 50 mM [Tollens'] (Figure S2 in the Supporting Information). In contrast to AgNP@**2**, the formation of AgNPs using ligand **3** was dependent on the reaction conditions. TEM analysis of several examples in this series produced angular AgNP@**3** of tuneable sizes that ranged from (12 ± 3) nm in diameter when a higher concentration of Tollens' was used (#31, Figure S3c in the Supporting Information) through to (33 ± 7) nm when an intermediate concentration of Tollens' was used (#19, Figure S3a). Lower concentrations of Tollens' did not form AgNPs@**3**. No silver mirrors or formation of Ag aggregates were observed when ligand **3** was used. This suggests that the third galactose sugar present in **2** is not essential for AgNP formation.

A narrow reaction window was observed for the formation of poor quality and polydisperse AgNPs using ligand **4** (i.e., AgNP@**4**). Yellow samples with comparatively weak plasmon peaks (maximum absorption at 0.1) were formed at [Tollens'] 100 μM to 1 mM with silver mirrors and aggregates predominating outside the optimal conditions (Figure S4a in the Supporting Information, grey boxes). The poor dispersity and size control of AgNP@(**4**) was confirmed by SEM analysis (Figure S5 in the Supporting Information).

AgNPs formed using ligand **5** (i.e., AgNP@**5**) displayed a significantly weaker dependence on [Tollens'] (Figure S6a in the Supporting Information) than that observed for **3**. A similarly weak dependence on AgNP formation was previously observed using ligand **25**, which produced angular (10 ± 2) nm AgNP@**25** over a similarly wide concentration range of [**25**] and [Tollens']. AgNP@**5** was formed with diameters that ranged from (12 ± 1) nm (#22, Figure S7a in the Supporting Information) to (20 ± 2) nm (#28, Figure S7d).

The formation of AgNPs was then investigated by using ligand **6** and Tollens' reagent in the presence of three equivalents of galactose (Figure S8a in the Supporting Information). This experiment was conducted to determine whether covalent attachment of the reducing sugars to the central ligand core was essential to facilitate AgNP forma-

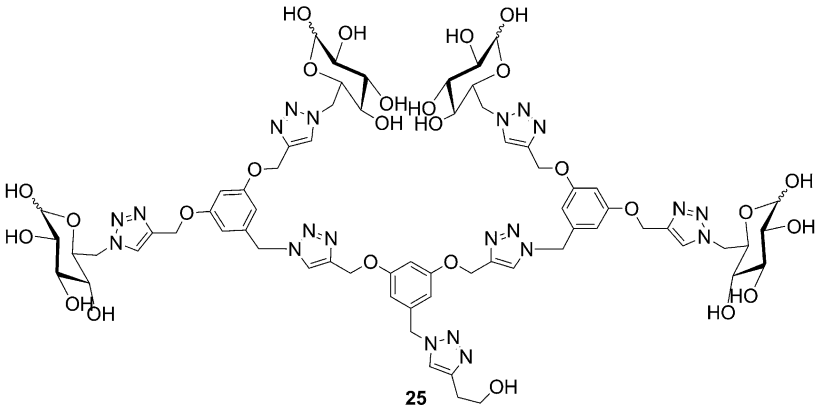

25

tion. A ratio of galactose/**6** (3:1) was chosen because this correlated to the same stoichiometry of reducing sugars in **2**. No AgNPs were formed over all concentrations of **6** and Tollens' surveyed. We therefore conclude that covalent attachment of galactose sugars to the triazole scaffold is essential for these ligands to facilitate AgNP formation. Table 1 summarises the results of AgNPs formed in this study.

Table 1. Summary of AgNPs formed using ligands **2**, **3** and **5**.

Ligand	Tollens'/ligand	AgNP size [nm]
2	1 mM:1 mM (1:1)	21 ± 3
	10 mM:25 mM (2:5)	17 ± 3
	50 mM:25 mM (2:1)	18 ± 5
3	10 mM:25 mM (2:5)	33 ± 7
	20 mM:1 mM (20:1)	14 ± 3
	50 mM:25 mM (2:1)	12 ± 3
5	20 mM:1 mM (20:1)	12 ± 1
	20 mM:10 μM (2000:1)	15 ± 2
	50 mM:5 mM (10:1)	13 ± 2
	50 mM:100 μM (500:1)	20 ± 2

The Kinetics of AgNP Formation

The kinetics of AgNP formation was then explored using **2**–**5** by monitoring the onset of the surface plasmon peak at 400 nm. The onset of formation of AgNP@(**2**) was observed at approximately 180 s with an end point at approximately 420 s using 100 μM [**2**] and 10 mM [Tollens'] (Figure 4). A similar kinetic profile was observed for the formation of AgNP@**4** using 500 μM [**4**] and 5 mM [Tollens']. A similar rate of onset of formation of AgNP@**3** was also observed but with a slower end point (ca. 570 s) using 100 μM [**3**] and 10 mM [Tollens']. The most significant difference in the kinetics of AgNP formation was observed for AgNP@**5**. A slower rate of onset (ca. 192 s) and a significantly slower end point (ca. 1200 s) was observed for the formation of AgNP@**5** using 100 μM [**5**] and 10 mM [Tollens'].

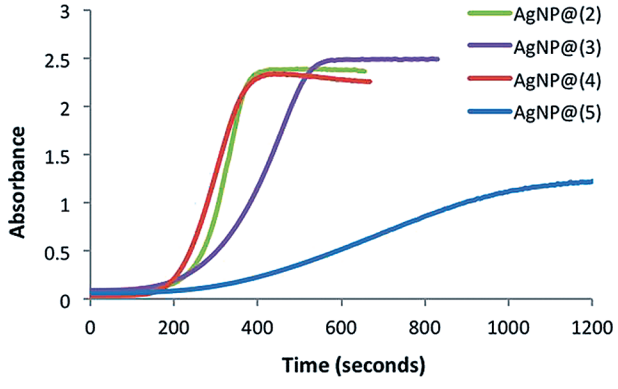

Figure 4. Kinetics of formation of AgNP using **2** (green), **3** (purple), **4** (red) and **5** (blue) as monitored by the formation of the surface plasmon peak at 400 nm.

AgNPs Formed Using Ligand 5 are Stable in High-Salt Buffers

The stability of AgNP@**2** and AgNP@**5** in aqueous solutions that contain NaCl was then monitored. AgNP@**2** remained dispersed in aqueous solutions up to 0.3 M NaCl (Figure S9a in the Supporting Information), whereas AgNP@**5** remained dispersed in 4.5 M NaCl at room temperature over a period of 24 hours (Figure S9b). We conclude that the larger ligand (**5**) significantly enhances the stability of AgNP colloid in high-salt buffer solutions.

Binding Characteristics of Ligands with Ag^I

^{1}H NMR Spectroscopic Titration Studies

An ^{1}H NMR spectroscopic titration study using ligands **1**–**3** and **6**–**7** in the presence of up to six equivalents of $AgNO_3$ was conducted to gain further insight into the Ag^I-binding characteristics. Previous work revealed a large downfield shift (δ = 0.2 ppm) for both H^c and H^d in **1** upon the addition of one equivalent of Ag^I.[23] This downfield shift of H^d reached a maximum at an Ag^I/**1** ratio of 1:1, whereas the downfield shift of H^c reached its maximum at a 2:1 Ag^I/**1** ratio. This suggested that in the presence of one equivalent of Ag^I, all three triazole units were participating in the coordination of a single Ag^I cation. A further increase in Ag^I changed the chelating behaviour of **1** to possibly access a putative binuclear metallocyclic species as observed with previous Ag^I-chelating triazole ligands.[30–32]

Triazole protons (H^f) and aromatic protons (H^g) of **2** were used as diagnostic markers of Ag^I coordination (Figure S10 in the Supporting Information). Titration of up to one equivalent of Ag^I resulted in a significantly smaller downfield shift (δ = 0.04 ppm) of H^f relative to that observed for H^c/H^d in **1** (Figure S10d). A further marked divergence in the Ag^I-chelating behaviour between **1** and **2** was the observation of a further δ = 0.08 ppm downfield shift of H^f in **2** upon the addition of six equivalents of Ag^I. In contrast to the behaviour of H^f in **2**, a δ = 0.16 ppm upfield shift of the aromatic H^g was observed upon the addition of up to three equivalents of Ag^I (Figure S10f). This behaviour is divergent from the initial upfield shift of the aromatic H^e in **1**, which was followed by the chemical shift of H^e returning to its original position after the addition of six equivalents of Ag^I. We therefore conclude that the Ag^I-binding affinity of **2** is weaker and markedly different to **1**.

An ^{1}H NMR spectroscopic titration was then conducted using ligand **3**. A similar Ag^I-chelating behaviour to **2** was

observed using triazole H^h/H^j and aromatic protons H^i of **3** as diagnostic markers of Ag^I coordination (Figure S11 in the Supporting Information). Titration of up to one equivalent of Ag^I resulted in a downfield shift (δ = 0.04 ppm) of H^h/H^j, similar to that observed for H^f in **2** (Figure S11d,f). A further δ = 0.1 ppm downfield shift was observed up to the addition of six equivalents of Ag^I. A δ = 0.18 ppm upfield shift of the aromatic H^i was observed upon the addition of up to three equivalents of Ag^I (Figure S11h), again consistent with that observed for H^g in **2**.

To compare the differences in Ag^I binding of the two core scaffolds in more detail, ^{1}H NMR spectroscopic titrations were conducted by using **6** and **7**. Ligand **6** is representative of the basic core of the second-generation ligand **2**, whereas **7** is representative of the first-generation ligand (**1**). Figures S12 and S13 in the Supporting Information show a comparative analysis of the Ag^I-binding characteristics of ligand **6** and **7** by ^{1}H NMR spectroscopic titration with $AgNO_3$. Titration of up to one equivalent of Ag^I resulted in a δ = 0.04 ppm downfield shift of H^k in **6**. A further δ = 0.1 ppm downfield shift was observed upon the addition of a further three equivalents of Ag^I (Figure S12d). For ligand **7**, titration of up to one equivalent of Ag^I, a δ = 0.06 ppm downfield shift of H^m and a δ = 0.02 ppm downfield shift of H^o was observed. A further downfield shift of δ = 0.1 ppm in H^m and δ = 0.07 ppm in H^o occurred upon the addition of a further three equivalents of Ag^I (Figure S13d,f). A δ = 0.2 ppm upfield shift of the aromatic protons of both ligands was observed upon the addition of up to three equivalents of Ag^I (Figure S12f and S13h). We conclude that **6** and **7** bind to Ag^I in a similar manner.

Calculation of the Ag^I-Binding Constant

The binding affinity of Ag^I for ligands **1**–**3** and **6**–**7** was then calculated by nonlinear least-squares fitting (Table 2). The acquired ^{1}H NMR spectroscopic data of the downfield shift observed for the triazole protons of **1**–**3** and **6**–**7**, and the concentration of the Ag^I was used to calculate the Ag^I-binding constants using the WinEQNMR2 software (Figure S14 in the Supporting Information).[33] The ligand that exhibited the highest affinity when one equivalent of Ag^I was added was **1** with a binding constant of (72393 ± 2) M^{-1}. This is two orders of magnitude higher than the binding constants calculated for ligands **2**–**7**. An interesting observation was the third galactose sugar in the southernmost part of ligand **2** [(533 ± 1) M^{-1}] has a slightly detrimental effect on Ag^I binding relative to **3** [(743 ± 1) M^{-1}]. The higher binding constant of **6** [(794 ± 1) M^{-1}] relative to **7** [(489 ± 1) M^{-1}] was also unexpected and shows that the core structure of the second-generation ligands (i.e., **2** and **3**) have a higher affinity for Ag^I than the core of **1**. When the galactose sugars replaced aliphatic alcohol chains (i.e., **7**→**1**), the binding affinity increased massively, whereas only a moderate increase in binding affinity was observed when the structure was changed from **6**→**3**. The significant reduction in Ag^I-binding affinity of **7** relative to ligand **1** suggests that the two northernmost galactose sugars in **1** collectively enhance Ag^I binding.

Table 2. Ag^I-binding affinity of ligands **1**–**3** and **6**–**7** calculated by nonlinear curve fitting of ^{1}H NMR spectroscopic chemical-shift data of the triazole protons using the WinEQNMR2 software program.

Compound	K_a [M^{-1}]	log K_a
1	72393 ± 2	4.859 ± 0.219
2	533 ± 1	2.727 ± 0.018
3	743 ± 1	2.871 ± 0.040
6	794 ± 1	2.900 ± 0.057
7	489 ± 1	2.689 ± 0.012

Mass Spectrometric Analysis of the Ag^I Binding Using Ligands 2, 3 and 5

ESI-MS analysis of **2** in complex with one equivalent of Ag^I resulted in the predominant formation of the $[M + Ag]^+$ ion (*m*/*z* 962). A minor amount of the 2:1 **2**/Ag^I complex $[2M + Ag + H]^+$ at *m*/*z* 1819 (Figure S15a in the Supporting Information) was observed, which was indicative of the formation of a metallocyclic species.[30–32] The $[M + Ag]^+$ ion still predominated in the presence of two equivalents of Ag^I; however, the formation of a small amount of $[M + 2Ag]^+$ at *m*/*z* 1070 was also observed (Figure S15b). Increasing the number of equivalents of Ag^I up to four afforded a range of ions that corresponded to $[M + Ag]^+$, $[M + 2Ag]^+$ and $[M + 3Ag]^+$, but with the 1:1 complex still predominating (Figure S15d). Thus, in the presence of one equivalent of Ag^I, ligand **2** predominantly forms the **2**·Ag^I complex with a 1:1 stoichiometry. Increasing the number of equivalents of Ag^I resulted in the formation of a range of other minor Ag^I-chelating species.

ESI-MS analysis of the Ag^I-chelating properties was then investigated using ligand **3**. A molecular ion $[M + Na]^+$ with *m*/*z* 774 was the predominant species when one equivalent of Ag^I was added to **3**. A minor amount of $[M + Ag]^+$ at *m*/*z* 860 was also observed (Figure S16a in the Supporting Information). The $[M + Ag]^+$ peak was the predominant species in the presence of two equivalents of Ag^I (Figure S16b). As the number of equivalents of Ag^I was increased up to four, the $[M + Ag]^+$ ion still predominated with the formation of a small amount of $[M + 2Ag]^+$ at *m*/*z* 966 and a complete loss of $[M + Na]^+$ at *m*/*z* 774 (Figure S16d).

ESI-MS analysis of the Ag^I-chelating properties was then carried out by using ligand **5**. The major molecular ion was *m*/*z* 1205, which corresponded to $[M + 2Ag]^{2+}$ when one equivalent of Ag^I was added to **5**. A series of other minor adducts was also observed in the mixture, such as *m*/*z* 2303 $[M + Ag]^+$ and 839 $[M + 3Ag]^{3+}$ (Figure S17a in the Supporting Information). The wide range of molecular ions observed in this ligand complex was in stark contrast to the predominant $[M + Ag]^+$ observed in the 1:1 **2**·Ag^I complex. As the number of equivalents of Ag^I was increased from one up to six, the $[M + 3Ag]^{3+}$ peak became more pronounced (Figure S17d). At 7.5 equiv. of Ag^I, $[M + 3Ag]^{3+}$ was the dominant peak in the spectrum with a complete loss of $[M + Ag]^+$ at *m*/*z* 2303 (Figure S17e). In summary, the Ag^I-binding behaviour of ligand **5** diverges quite mark-

edly from **2** and **3** by its ability to chelate a much wider dynamic range of Ag^I ions. This Ag^I binding behaviour also varies according to the stoichiometric ratio of ligand **5**.

Discussion

These experiments were designed to test how the structural features of triazole ligands influenced the size, morphology, stability and dispersity of AgNPs. We discuss here several conclusions that have emerged from our results.

The Size of AgNPs Formed Using Ligand 3 is Inherently Tunable

Ligand **1** has an Ag^I-binding affinity 136 times higher than ligand **2** and 97 times higher than ligand **3** (Table 2). As a consequence of this significantly higher Ag^I-binding affinity, the rate of nucleation of **1** (120 s)[23] is faster than in **2** (180 s). We speculate that while this increase in binding affinity in **1** increases the rate of Ag nucleation, the rate of growth of these nuclei into AgNP@**1** slows relative to AgNP@**2** as reflected by the longer endpoint of **1** (588 s)[23] relative to **2** (420 s). In the case of AgNP@**1**, we assume that the increase in Ag^I-binding affinity would produce a larger population of Ag nuclei in complex with **1** relative to **2** in the initial nucleation stages; however, once these nuclei are formed, the rate of growth of these nuclei into AgNPs slows. It is not clear at present if this slower growth rate is directly related to the binding affinity of Ag clusters to these ligands, and this aspect will be a subject of further investigation.

A significant difference in AgNP formation that we observed in this study relative to our previous study was the inherent tunability of the size of AgNP@**3** relative to AgNP@**1**. In the case of AgNP@**3**, monodispersed angular AgNPs were produced with diameters that ranged from (12 ± 3) up to (33 ± 7) nm (Figure S3), whereas AgNP@**2** produced angular NPs that were typically approximately 18 nm in diameter (Figure 3). Crucially, the diameters of these AgNPs were dependent on the concentration of the Tollens' reagent and the ligand used. This behaviour was not observed when ligand **1** was used to form AgNP@**1**. In this case, only spherical AgNPs with a significantly smaller diameter of (8 ± 5) nm were formed over a wide range of [ligand] and [Tollens']. We attribute the lack of tunability of the size of AgNP@**1** and the differences in shape to the higher Ag^I-binding affinity of **1** and the different Ag^I-chelating behaviour of this ligand than AgNP@**3**. An unexpected result was the ability to tune the size of AgNP@**2** relative to AgNP@**3**. A possible explanation for this is that the presence of the third galactose sugar in the southern part of ligand **2** perturbs size tunability.

The Ag^I Binding Affinity is Sensitive to Ligand Structure

Another unexpected result that arose from this study was the significant difference in Ag^I-binding affinity of **1** than with **7**. Both ligands contain the same core structure. When the northeast and northwest triazoles comprise an alkyl chain and a primary alcohol (i.e., **7**), there is a significant reduction in Ag^I-binding affinity than when a galactose is installed in this position. This result suggests that these sugars contribute to Ag^I binding although the nature of this interaction is unclear at present. We showed that ligand **26** prepared in our previous study did not facilitate the formation of AgNPs and produced Ag aggregates instead.[23] This indicates that the southern triazole is essential in facilitating AgNP formation. Further structural studies will be required to understand the role of these galactose sugars in enhancing Ag^I binding.

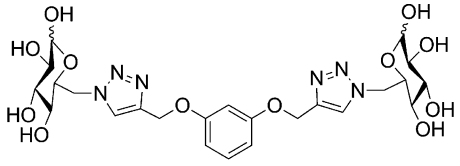

26

Changing the southern ligand core from **1** to **2/3** also resulted in a significant reduction in Ag^I binding. This was unexpected as ligands **2** and **3** retain the same features in the northern part of the structure as **1** and provides further justification that the southern half of the structure plays just as significant a role in tuning the Ag^I-binding affinity as the galactose sugars in the northern part of the structure. The installation of a third galactose in **2** resulted in a slightly weaker Ag^I-binding affinity (533 M^{-1}) relative to the Ag^I-binding affinity of **3** (743 M^{-1}). There was some Ag mirror formation observed when the reaction conditions of AgNP@**2** were surveyed (e.g., #21, #27 and #33; Figure 2). The formation of Ag mirrors was not observed when ligand **3** was used, thus suggesting that the covalent attachment of a third galactose in the southern part of these ligands actually has a detrimental effect on the formation of AgNP@**3**. Kinetic studies revealed a similar rate of onset of AgNP@**2** and AgNP@**3**, but the end point for **3** was slower (570 s) than **2** (420 s; Figure 4). Thus we infer that the southernmost galactose does increase the rate of AgNP formation. However, at certain [**2**] and [Tollens'], the southernmost galactose sugar destabilises the growth of AgNP formation and can result in Ag mirrors under certain conditions. Taken collectively, our results suggest that merely increasing the number of reducing equivalents (i.e., the number of galactose units) in the system does not necessarily equate to the formation of monodispersed AgNPs with smaller diameters.

Larger Triazole Ligand 5 Formed Highly Stable Monodisperse AgNPs

Out of all the ligand systems surveyed, ligand **5** produced the most stable suspensions in high-salt buffers. Furthermore, this ligand facilitated the formation of angular AgNP@**5** over much wider concentration ranges of [ligand] and [Tollens'] than to ligands **2** and **3** (Figure S6a). A lack

of size tunability in the formation of AgNP@**5** was also observed in the formation of AgNP@**25** and suggests that the addition of the first-generation triazole ligands on the distal ends in **5** tends to override the influence of the central phloroglucinol core. An extremely long end point of AgNP@**5** formation relative to **2** and **3** was also observed. This could be a contributing factor to the slightly larger observed size of AgNP@**5** than AgNP@**1** and AgNP@**25**. Taken collectively, compound **5** is a highly versatile ligand that can be used to form size-selected, angular and stable suspensions of AgNPs in high-salt buffers.

Conclusion

In this study, we have shown for the first time that the structure and the Ag^I-binding affinity of triazole ligands plays a defining role in controlling the size and shape of AgNPs formed using the Tollens' reagent as an Ag^I source. Ligands that display weaker Ag^I-binding affinity (i.e., **2** and **3**) produced angular AgNPs that were larger in diameter than spherical AgNPs prepared by using ligand **1** with high Ag^I-binding affinity. The methodology described herein could therefore facilitate the application of size- and shape-tunable AgNPs in areas such as drug delivery, imaging, diagnostics and optoelectronics. Efforts are now underway to investigate the application of this methodology in these areas and will be reported in due course.

Experimental Section

For detailed experimental information see the Supporting Information.

Supporting Information (see footnote on the first page of this article): Details on the synthesis of triazole ligands, protocols for the synthesis and characterisation of AgNPs, kinetics studies of AgNP formation and the calculation of Ag-binding affinities of triazole ligands.

Acknowledgments

The Engineering and Physical Sciences Research Council (EPSRC) is thanked for an Advanced Research Fellowship (to G. A. B., grant number EP/E055095/1) and for a postgraduate studentship (to A. J. F.). H. A. K. thanks the University of King Abdulaziz in Saudi Arabia for a postgraduate studentship. A. W. C. thanks the Royal Academy of Engineering (grant number 10216/103), the James Watt Nanofabrication Centre, and the Kelvin Nanocharacterisation Centre at the University of Glasgow. A. J. F. also thanks the University of Leicester for a postgraduate studentship. The authors thank Ishwar Singh for assistance in the analysis of NMR spectra.

[1] J. N. Anker, W. P. Hall, O. Lyandres, N. C. Shah, J. Zhao, R. P. Van Duyne, *Nature Materials* **2008**, *7*, 442.
[2] T. Shegai, S. Chen, V. D. Miljkovic, G. Zengin, P. Johansson, M. Kall, *Nature Commun.* **2011**, *2*.
[3] M. D. Malinsky, K. L. Kelly, G. C. Schatz, R. P. Van Duyne, *J. Am. Chem. Soc.* **2001**, *123*, 1471.
[4] C. Dose, D. Ho, H. E. Gaub, P. B. Dervan, C. H. Albrecht, *Angew. Chem. Int. Ed.* **2007**, *46*, 8384; *Angew. Chem.* **2007**, *119*, 8536.
[5] J. Zheng, P. R. Nicovich, R. M. Dickson, *Annual Review of Physical Chemistry*, Annual Reviews, Palo Alto, **2007**, vol. 58, p. 409.
[6] S. Lal, N. K. Grady, J. Kundu, C. S. Levin, J. B. Lassiter, N. J. Halas, *Chem. Soc. Rev.* **2008**, *37*, 898.
[7] C. L. Nehl, J. H. Hafner, *J. Mater. Chem.* **2008**, *18*, 2415.
[8] A. W. Clark, J. M. Cooper, *Angew. Chem. Int. Ed.* **2012**, *51*, 3562; *Angew. Chem.* **2012**, *124*, 3622.
[9] M. Rycenga, C. M. Cobley, J. Zeng, W. Li, C. H. Moran, Q. Zhang, D. Qin, Y. Xia, *Chem. Rev.* **2011**, *111*, 3669.
[10] L. S. Nair, C. T. Laurencin, *J. Biomed. Biotechnol.* **2007**, *3*, 301.
[11] K. Belser, T. Vig Slenters, C. Pfumbidzai, G. Upert, L. Mirolo, K. M. Fromm, H. Wennemers, *Angew. Chem. Int. Ed.* **2009**, *48*, 3661; *Angew. Chem.* **2009**, *121*, 3715.
[12] H. Wennemers, *J. Pept. Sci.* **2012**, *18*, 437.
[13] G. Upert, F. Bouillere, H. Wennemers, *Angew. Chem. Int. Ed.* **2012**, *51*, 4231; *Angew. Chem.* **2012**, *124*, 4307.
[14] M. Hanisch, M. Mackovic, N. Taccardi, E. Spiecker, R. N. K. Taylor, *Chem. Commun.* **2012**, *48*, 4287.
[15] R. S. Patil, M. R. Kokate, C. L. Jambhale, S. M. Pawar, S. H. Han, S. S. Kolekar, *Adv. Nat. Sciences Nanosci. Nanotechnol.* **2012**, *3*, 015013.
[16] Y. D. Yin, Z. Y. Li, Z. Y. Zhong, B. Gates, Y. N. Xia, S. Venkateswaran, *J. Mater. Chem.* **2002**, *12*, 522.
[17] L. Kvitek, M. Vanickova, A. Panacek, J. Soukupova, M. Dittrich, E. Valentova, R. Prucek, M. Bancirova, D. Milde, R. Zboril, *J. Phys. Chem. C* **2009**, *113*, 4296.
[18] J. Soukupova, L. Kvitek, A. Panacek, T. j. Nevecna, R. Zboril, *Mater. Chem. Phys.* **2008**, *111*, 77.
[19] L. Kvitek, A. Panacek, J. Soukupova, M. Kolar, R. Vecerova, R. Prucek, M. Holecova, R. Zboril, *J. Phys. Chem. C* **2008**, *112*, 5825.
[20] A. Panacek, L. Kvitek, R. Prucek, M. Kolar, R. Vecerova, N. Pizurova, V. K. Sharma, T. j. Nevecna, R. Zboril, *J. Phys. Chem. B* **2006**, *110*, 16248.
[21] L. Kvitek, R. Prucek, A. Panacek, R. Novotny, J. Hrbac, R. Zboril, *J. Mater. Chem.* **2005**, *15*, 1099.
[22] Y. Saito, J. J. Wang, D. N. Batchelder, D. A. Smith, *Langmuir* **2003**, *19*, 6857.
[23] R. Dondi, W. Su, G. A. Griffith, G. Clark, G. A. Burley, *Small* **2012**, *8*, 770.
[24] W. E. Benet, G. S. Lewis, L. Z. Yang, D. E. P. Hughes, *J. Chem. Res.* **2011**, 675.
[25] V. K. Sharma, R. A. Yngard, Y. Lin, *Adv. Colloid Interface Sci.* **2009**, *145*, 83.
[26] P. Wu, A. K. Feldman, A. K. Nugent, C. J. Hawker, A. Scheel, B. Voit, J. Pyun, J. M. J. Frechet, K. B. Sharpless, V. V. Fokin, *Angew. Chem. Int. Ed.* **2004**, *43*, 3928; *Angew. Chem.* **2004**, *116*, 4018.
[27] G. A. Burley, J. Gierlich, M. R. Mofid, H. Nir, S. Tal, Y. Eichen, T. Carell, *J. Am. Chem. Soc.* **2006**, *128*, 1398.
[28] I. Mallard-Favier, P. Blach, F. Cazier, F. Delattre, *Carbohydr. Res.* **2009**, *344*, 161.
[29] P. Li, L. Wang, Y. Zhang, *Tetrahedron* **2008**, *64*, 10825.
[30] M. L. Gower, J. D. Crowley, *Dalton Trans.* **2010**, *39*, 2371.
[31] J. D. Crowley, P. H. Bandeen, L. R. Hanton, *Polyhedron* **2010**, *29*, 70.
[32] J. D. Crowley, P. H. Bandeen, *Dalton Trans.* **2010**, *39*, 612.
[33] M. J. Hynes, *J. Chem. Soc., Dalton Trans.* **1993**, 311.

Received: June 25, 2014
Published Online: August 15, 2014

